B-dot and D-dot sensors for (sub)nanosecond high-voltage and high-current pulse measurements

B-dot and D-dot Sensors for (Sub)Nanosecond High-Voltage and High-Current Pulse Measurements

T. Huiskamp, F. J. C. M. Beckers, E. J. M. van Heesch and A. J. M. Pemen

***Abstract*—In this paper, we present a large-bandwidth, high-current and high-voltage measuring system for pulse measurements in pulsed power systems. The developed sensors can be easily calibrated, require no extensive (3D) modeling, are very compact, are inexpensive, and have a bandwidth of up to several GHz. Moreover, they can be used in any pulsed power system where a pulse source is connected to its load by a coaxial cable (without disturbing the coaxial geometry).**

We developed this sensor system for use with our nanosecond pulse source system. The type of sensors we used are D-dot and B-dot sensors, which are compactly mounted on the coaxial cable that connects our nanosecond pulse source to its load. This enables us to measure the characteristics of each sensor very precisely with a vector network analyzer. With these characteristics — combined with the characteristics of the measuring cable assembly — we can numerically reconstruct the voltage and current waveforms that passed the sensor positions. Our calibration approach, the mounting on the coaxial cable and the post-processing of the results make these sensors very flexible. While we use the sensors for energy measurements, camera triggering and the general measurement of the pulses, other researchers can use these type of sensors as well in any system where a (coaxial) cable connects a pulse source to its load.

***Index Terms*—Sensors systems, high-voltage techniques, pulsed power systems, nanosecond pulses**

I. Introduction

SENSORS for high-voltage and high-current measurements are an essential ingredient for the successful operation of many pulsed power systems [1]. Unfortunately, commercially available current and voltage probes are expensive and often not suitable for all applications. When high bandwidths are required simultaneously with the need to measure high currents and high voltages, available probes can often not be used. For these applications, researchers construct their own current and/or voltage sensors. The advantages of these sensors are that they are relatively cheap, can be very accurate and can be designed such that they meet all the requirements for a particular measurement. However, a significant disadvantage of these homemade sensors is that the calibration can be difficult. This calibration often requires extensive (3D EM) modeling because no other sensors are available to verify if the signals from the homemade sensors are accurate. A further disadvantage is that these sensors only operate in a certain regime [2]. In this paper, we present a large bandwidth, high-current and high-voltage measuring system that can be easily calibrated, requires no (3D) modeling, is very compact, is inexpensive, and has a bandwidth of up to several GHz. Moreover, it can be used in any pulsed power system where a pulse source is connected to its load by a coaxial cable (without disturbing the coaxial geometry).

Manuscript received xx, 2015.

This work was supported by the Dutch Technology Foundation STW under contract number 10751.

T. Huiskamp, F. J. C. M. Beckers, E. J. M. van Heesch and A. J. M. Pemen are with the Electrical Energy Systems Group, Eindhoven University of Technology, 5600 MB Eindhoven, The Netherlands (e-mail: t.huiskamp@tue.nl; e.j.m.v.heesch@tue.nl; a.j.m.pemen@tue.nl).

A. Motivation

Recently, we designed and implemented an adjustable pulse duration (0.5–10 ns), adjustable output voltage (±0–50 kV), subnanosecond rise time (<200 ps) nanosecond pulse source for transient plasma generation [3]–[5]. We required large-bandwidth, high-current and high-voltage sensors for the measurement of the output pulses of the pulse source. These measurements would allow us to measure the plasma energy. Furthermore, using one of the sensor signals, we would obtain a reliable trigger for the camera with which we imaged the plasma on subnanosecond time scales [6]–[8].

The expected voltages and currents in the nanosecond pulse source system exceed 80 kV and 1 kA respectively at a rise time of several hundreds of picoseconds (several GHz bandwidth). Therefore, we faced the same challenge as many researchers before us: finding suitable sensors to measure these currents and voltages.

In pulsed-power technology a number of different types of sensors are generally used. For pulsed-power measurements, high-voltage probes and current sensors are commercially available [9]–[12]. However, these components are expensive and often not suitable for higher frequencies. Commercial current monitors are available up to several GHz bandwidth, but these systems can only measure a low current (up to several ampere). Furthermore, most of the commercially available components are bulky and cannot easily be implemented in compact setups. Therefore, homemade sensors such as D-I (Differentiating-Integrating) systems, capacitive voltage probes, Rogowski coils [13]–[18] or even electro-optic probes are often employed [19], [20].

Fast types of capacitive and inductive sensors are D-dot and B-dot sensors respectively [2], [21]–[23]. They are simple in design, can be made very compact and can measure large signals up to very high frequencies. It is these type of sensors that we will employ to measure the pulses from our nanosecond pulse source. The design of the D-dot and B-dot sensors that we present in this paper were motivated by the excellent results that were achieved with these type of designs in [22] and [2]. A first version of the D-dot version we developed was already presented in [4].

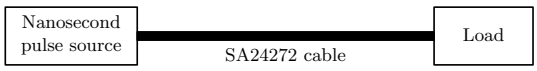

Fig. 1. A simplified representation of our nanosecond pulse source setup. The setup of many pulsed power systems is similar.

B. Paper Organization

After this introduction, we explain the principle of operation of the sensors in Section II, followed by their design in Section III and the complete measurement setup in Section IV. We then show an application example of the developed sensors in Section V. Finally, Section VI presents the conclusions.

II. Principle of Operation

A. Nanosecond Pulse Source Setup

Figure 1 shows a simplified version of our nanosecond pulse source setup. The nanosecond pulse source (presented in detail in [5]) is connected to its load (a plasma reactor) by a coaxial cable. Most pulsed power systems can be presented in this way, which reinforces our claim that the sensors that we present in this paper can be useful for many researchers.

The question is: where to place the sensors? At the source, on the cable, or at the load? Sensors are often placed at the source or at the load, but we already mentioned that calibration can then become difficult, especially at the high bandwidth we require. For instance, in [2] D-dot sensors were successfully placed inside the pulse forming line of a triaxial Blumlein-line nanosecond pulse source to monitor the pulse forming process. However, the researchers required extensive 3D EM modeling to calibrate the sensors. Furthermore, the pulses from that nanosecond pulse source had a rise time one order of magnitude longer than our pulses.

Because of the high-frequency nature of our pulses, reflections at the load will occur in the case of a load that is not perfectly matched. In our case, the load is a plasma reactor and is therefore unmatched. Placing sensors in the plasma reactor — thereby placing the sensors exactly where the reflections occur — makes the measurements difficult to unravel because the incoming pulse overlaps with the reflected pulse. In addition, the calibration of these sensors still require extensive modeling (because no other sensors exist to calibrate the homemade sensors with).

The significant advantage of our B-dot and D-dot sensors is that we mount them on the coaxial cable instead of in the source or the load. In this way, we can easily calibrate the sensors with a vector network analyzer (VNA). Therefore, we require no 3D EM modeling and obtain some important other advantages which we will point out in the next sections.

B. D-dot sensor

The D-dot sensor is a capacitively coupled electrode that measures the voltage created by the displacement current between the high-voltage electrode and the D-dot sensor electrode [2], [21]. This current is the derivative of the voltage on the high-voltage electrode.

In Section III we will show the design of the D-dot and B-dot sensors in detail. For the theoretical analysis in the next part it is only necessary to know that we placed the sensors in a compact metal body that is clamped onto the coaxial cable (a 50-Ω SA24272 cable[1] in our case). The sensors are made with SMA bulkhead connectors and couple to the inner electrode of the coaxial cable through small holes we made in the outer conductor of the cable.

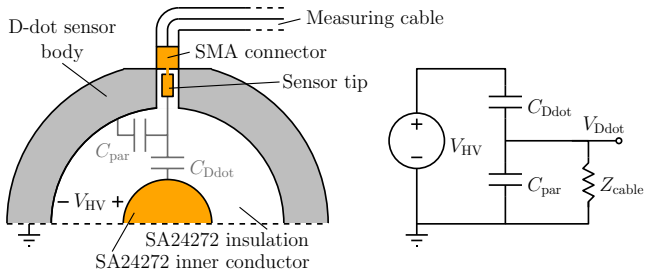

Fig. 2. A cut-away drawing of one of the D-dot sensors (compare with Fig. 4b and c) showing the equivalent electrical circuit. The circuit has a high-voltage part (C_{Ddot}) and a low-voltage part (C_{par} in parallel with Z_{cable}) which form a voltage divider.

Fig. 2 shows a sketch of the D-dot sensor in its metal body and the electrical equivalent circuit of the D-dot sensor system. Here V_{Ddot} is the voltage from the D-dot sensor, V_{HV} is the voltage on the inner conductor of the SA24272 cable, Z_{cable} is the impedance of the measuring cable, C_{par} is the parasitic capacitance from the D-dot sensor electrode to ground, and C_{Ddot} is the capacitance from the D-dot sensor electrode to the inner conductor of the SA24272 cable. This system is a voltage divider of which the impedance of the high-voltage part is

$$\frac{1}{j\omega C_{\mathrm{Ddot}}} \tag{1}$$

and the impedance of the low-voltage part is

$$\frac{Z_{\mathrm{cable}}}{j\omega Z_{\mathrm{cable}} C_{\mathrm{par}} + 1}. \tag{2}$$

The transfer function of the system $H_{\mathrm{Ddot}}(j\omega)$ then becomes

$$H_{\mathrm{Ddot}}(j\omega) = \frac{V_{\mathrm{Ddot}}}{V_{\mathrm{HV}}} = \frac{j\omega Z_{\mathrm{cable}} C_{\mathrm{Ddot}}}{j\omega Z_{\mathrm{cable}}(C_{\mathrm{Ddot}} + C_{\mathrm{par}}) + 1}. \tag{3}$$

Usually, D-dot sensors are operated either in a regime where $j\omega Z_{\mathrm{cable}}(C_{\mathrm{Ddot}} + C_{\mathrm{par}}) \gg 1$ or in a regime where $j\omega Z_{\mathrm{cable}}(C_{\mathrm{Ddot}} + C_{\mathrm{par}}) \ll 1$. In the first regime (high frequency) the output voltage of the D-dot sensor is proportional to V_{HV}. This regime is generally called the self-integrating regime [26], [27]. In the second regime (low frequency) the output voltage of the D-dot sensor is proportional to $\frac{dV_{\mathrm{HV}}}{dt}$. This regime is called the differentiating regime. In most cases, D-dot sensors are designed in such a way that they operate in one of these two regimes because then the measurements can be easily converted to the high-voltage signal with either a passive integrator and a calibration factor for the differentiating sensor, or just a calibration factor for the

[1]The SA24272 cable was manufactured by Suhner (later Huber-Suhner). It was used at Eindhoven University of Technology at the end of the 1980s and the beginning of the 1990s for low-loss signal transport [24], [25]. A technical data sheet of the SA24272 cable is included as an appendix in [24]. A comparable cable in today's market would be for instance the LMR-1700 cable from Times Microwave.

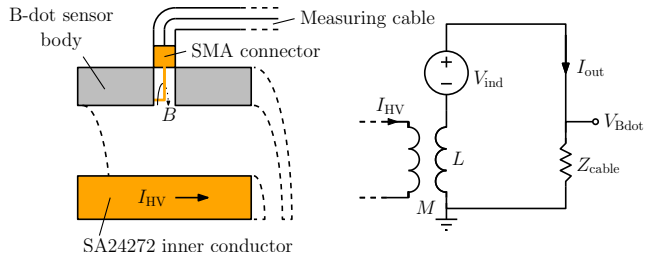

Fig. 3. Schematic representation of the B-dot sensor circuit (compare with Fig. 4b and d). The pulsed current I_{HV} generates a magnetic field which is partly picked up by the loop of the B-dot sensor. This induces a voltage in the sensor circuit.

self-integrating sensor. However, this puts design constraints on the sensors and requires thorough calculation, calibration and/or 3D EM simulations to design and operate the sensors. The advantage of our D-dot sensor is that it is mounted on a cable for which N-connectors are available. This allows us to precisely measure the transfer function with a VNA. This greatly simplifies the calibration of the sensors and ensures a very good calibration result, as we will show in Section IV-A.

C. B-dot sensor

A first implementation of the D-dot sensor was found to be suitable to measure the high-voltage pulses from the pulse source and served mainly as a "proof of concept" for this measuring technique and was presented in [4]. However, we also need to be able to measure the current associated with the high-voltage pulses to be able to measure the power and the energy of the pulse. Especially in plasma experiments is crucial to know how much energy is dissipated by the plasma. A suitable sensor to measure the current is the B-dot sensor [22], [23].

The B-dot sensor is an inductively coupled sensor. It is a small loop which picks up part of the magnetic field that is generated by the pulse as it passes the sensor position. The loop is again connected to an SMA bulkhead connector (see Section III).

Fig. 3 shows a sketch of the B-dot sensor in its metal body and the electrical equivalent circuit of the B-dot sensor system. Here V_{Bdot} is the voltage from the B-dot sensor, I_{HV} is the current through the inner conductor of the SA24272 cable, V_{ind} is the induced voltage along the B-dot electrode, I_{out} is the current in the B-dot sensor electrode, Z_{cable} is the impedance of the measuring cable, L is the inductance of the B-dot sensor electrode, and M is the mutual inductance between the B-dot sensor electrode and the conductors of the SA24272 cable. The induced voltage in the B-dot sensor is

$$V_{\mathrm{ind}} = M\frac{dI_{\mathrm{HV}}}{dt}. \tag{4}$$

Furthermore, we have

$$V_{\mathrm{Bdot}} = I_{\mathrm{out}} Z_{\mathrm{cable}}. \tag{5}$$

The equation that describes the equivalent circuit of the B-dot sensor is found by applying the Kirchhoff voltage law:

$$M\frac{dI_{\mathrm{HV}}}{dt} = L\frac{dI_{\mathrm{out}}}{dt} + Z_{\mathrm{cable}} I_{\mathrm{out}}. \tag{6}$$

From this equation the transfer function of the B-dot sensor is found as

$$H_{\mathrm{Bdot}}(j\omega) = \frac{V_{\mathrm{Bdot}}}{I_{\mathrm{HV}}} = \frac{j\omega M}{j\omega\frac{L}{Z_{\mathrm{cable}}} + 1}. \tag{7}$$

From this equation we see that the B-dot sensor is self-integrating when $j\omega\frac{L}{Z_{\mathrm{cable}}} \gg 1$ and that it is working in the differentiating regime when $j\omega\frac{L}{Z_{\mathrm{cable}}} \ll 1$. Just as with the D-dot sensor, it is not important in which regime our B-dot operates because we can measure the entire transfer function directly with the VNA.

III. Design

To be able to measure voltage and current at the same position, we integrated two B-dot sensors and two D-dot sensors into the same sensor body. The reason we used two sensors of each type in the sensor body is to increase the signal-to-noise ratio of the measurements. Small amounts of oscilloscope noise will be integrated during the numerical processing of the data and will result in low-frequency oscillations and offsets which are difficult to remove. With two sensors capturing the same signal, we can average the results and the noise will be halved, resulting in a cleaner output signal.

Besides oscilloscope noise we will experience some small amount of interference from the experiment itself. This is present as a common-mode signal on the measuring cables which — despite numerous precautions — proves difficult to remove altogether. In the case of the D-dot sensors this problem is solved by increasing the sensor area and thus increasing the output voltage of the sensors (while retaining the same level of interference). The disadvantage of this method is that besides increasing C_{Ddot}, C_{par} will also increase. This results in a lower cut-off frequency above which the sensor will start to behave as a self-integrating sensor. Here the flexibility of our approach becomes apparent because we are able to measure the entire transfer function with the VNA and are able to correct for it in the frequency domain. Therefore, a sensor that works both in the differentiating and the self-integrating regime is not a problem for our method.

For the B-dot sensors, the problem of interference is solved by an opposite orientation of the second B-dot sensor. This results in a positive output voltage on the first B-dot sensor and a negative output voltage on the second B-dot sensor when a pulse passes. We then subtract the signals to obtain an output signal with half the oscilloscope noise and no interference (the interference from both sensors cancels).

Figure 4 shows the sensor body. It is a brass body and can be mounted onto the SA24272 cable by a clamping mechanism. The D-dot sensors consist of a metal electrode soldered onto the tip of an SMA bulkhead connector (shown in Fig. 4b and c). The B-dot sensors consist of metal loops soldered on one end onto the tip of an SMA connector and on the other end to the metal body (shown in Fig. 4b and d). Figures 4e and f show the holes in the outer conductor of the coaxial cable and the way the sensor body is clamped onto the cable respectively.

The tips of the two D-dot sensors are bigger than the first implementation in [4] to achieve a higher output voltage and thereby decrease the influence of experimental interference.

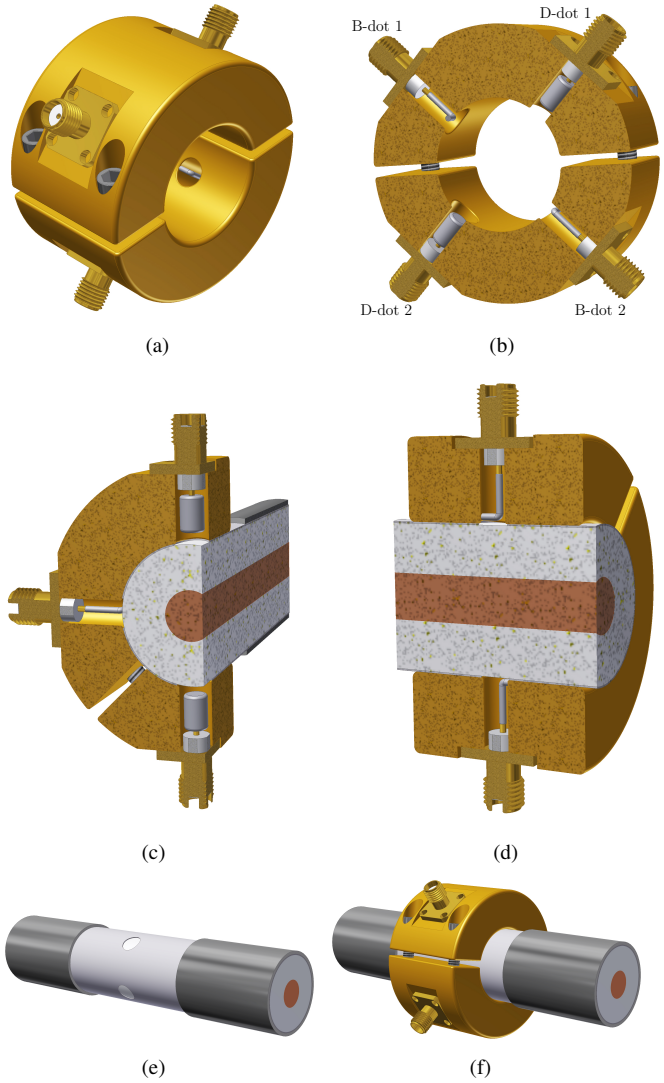

Fig. 4. (a) The sensor body with two D-dot sensors and two B-dot sensors. (b) Cut-away drawing of the sensor body with the D-dot and B-dot sensors indicated. (c) A view of the D-dot sensor. The sensor electrode is significantly larger than in the previous D-dot sensor of [4]. (d) A view of the B-dot sensor. It is a small loop that picks up part of the magnetic field generated by the nanosecond pulse. (e) The holes that we made in the outer conductor of the SA24272 cable to fit the sensors. (f) The sensor body can be mounted on the SA24272 cable via a clamp construction.

The B-dot and D-dot sensors are mounted on the long SA24272 cable that is connected to the final implementation of the nanosecond pulse source. The cable is around 28 m long and connects the pulse source to the plasma reactor that is used in our plasma experiments (see [6]). The reason the cable is so long is to increase the transit time of the pulses, so that we can trigger a camera (which has an internal delay) in our plasma imaging experiments. On this cable we mounted three sensor bodies. Two bodies with two B-dot sensors and two D-dot sensors each and one body with just one B-dot sensor and one D-dot sensor. This last body is mounted at the output of the pulse source. It has only one sensor of each type because it will only be used to measure the voltage from the pulse source and not for energy measurements. The B-dot sensor in this body will be used to trigger the camera in our plasma

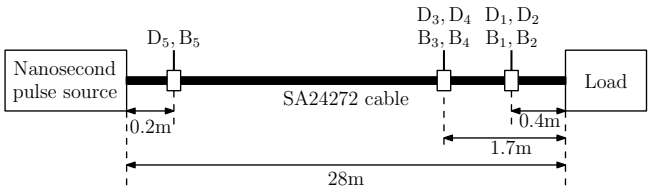

Fig. 5. The final sensor configuration. The sensor body with only one D-dot and B-dot sensor is placed at the pulse source side. The two sensor bodies with two D-dot and two B-dot sensors are placed near the load.

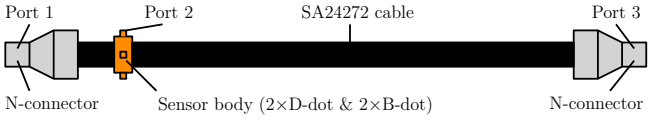

Fig. 6. Drawing of the calibration setup. The SA24272 cable is fitted with N-connectors so that it can be connected to the vector network analyzer. Port 2 of the network analyzer is connected to one of the sensors on the sensor body. The other sensors bodies are not shown in this drawing.

imaging experiments. The other two bodies are mounted near the load and can be used for plasma energy measurements. The entire sensor configuration is shown in Fig. 5.

IV. Measurement Setup

A. Calibration

We used a VNA to calibrate the B-dot and D-dot sensors and then used a reed-relay pulse source to verify the calibration. We calibrated the sensors before the SA24272 cable was installed into the nanosecond pulse source. We connected N-connectors to both sides of the SA24272 cable and connected them and the SMA connector of one of the sensors to a Rohde&Schwarz ZVB20 VNA. Fig. 6 shows to which ports of the VNA the cable assembly was connected. The transfer function of each sensor is now determined by measuring the S_{12}-parameters of the setup. We measured 1001 points in the frequency range of 10 MHz–4 GHz and averaged over 64 sweeps for each measurement. Since the sensor bodies are all close to either Port 1 or Port 3 (see Section IV-C) the dispersion in the SA24272 cable can be neglected (see the section on dispersion in the SA24272 cable in [3]).

Fig. 7 shows the results of the measurements. We measured the S-parameters of the sensors up to 4 GHz. The results show that all sensors operate partly in the differentiating regime and partly in the self-integrating regime in this frequency range. The lower frequency limit of the VNA is 10 MHz and it has a usable SNR (Signal to Noise Ratio) of about 90 dB. This explains the results below 100 MHz in Fig. 7.

Besides the measured amplitude of the S_{12} parameters, the figures also show the fitted transfer functions. We used Eq. 3 and 7 and a value of 50 Ω for Z_{cable} for the fitting. Table I shows the accompanying sensor parameters. Because of the lower frequency limit and the SNR of the VNA we will use the fitted transfer function in our measurements.

The differences between D-dot sensors D_1–D_4 are caused by slight differences in the sizes of the sensor heads and the mounting positions. The sensors are very sensitive for these minute differences. The same is true for B-dot sensors

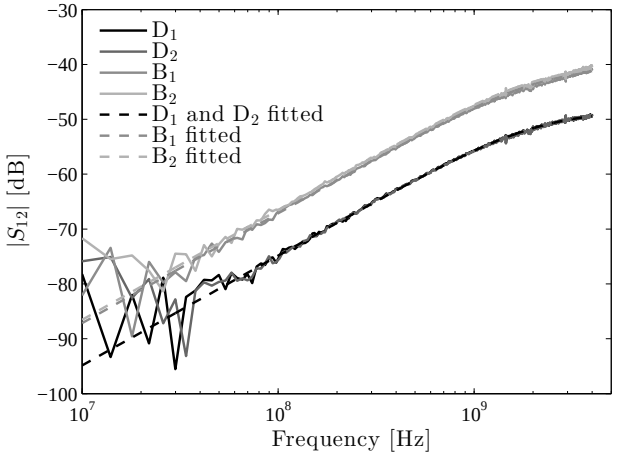

(a)

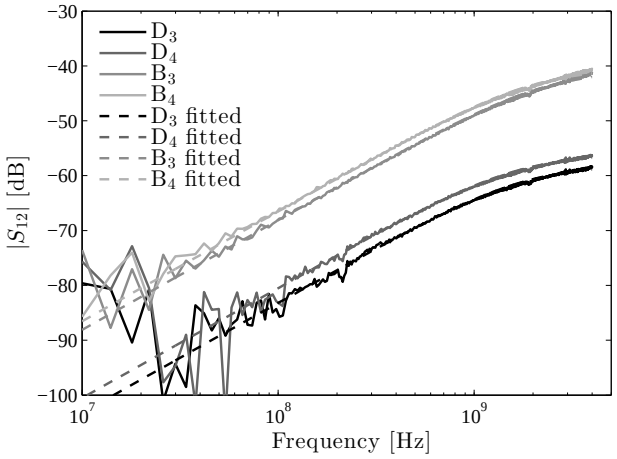

(b)

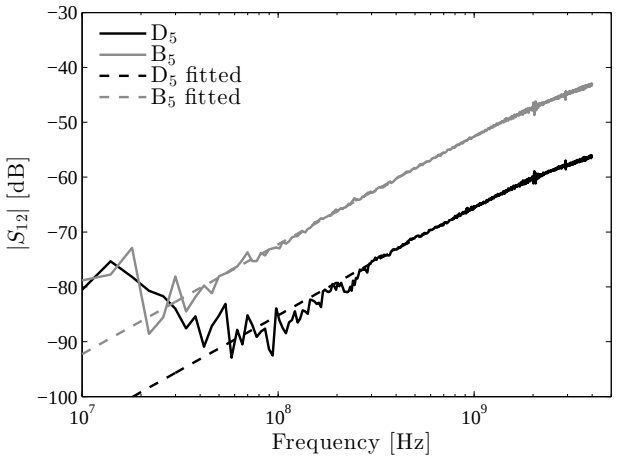

(c)

Fig. 7. Magnitude of S_{12} of the D-dot and B-dot sensor measurements and the fitted values for (a) D_1, D_2, B_1 and B_2, (b) D_3, D_4, B_3 and B_4, and (c) D_5 and B_5. (The artifact at around 2GHz in each transfer function turned out to be measuring artifact introduced by one of the cables we used to connect the SA24272 cable to the VNA.)

B_1–B_4. The differences between D-dot sensor D_5 and the rest and B-dot sensor B_5 and the rest result from a slightly different design. Here the advantage of our calibration method is very apparent: the slight geometrical differences between the individual sensors have no influence on the calibration

TABLE I
FITTED SENSOR PARAMETERS

D-dot	C_{Ddot}	C_{par}	B-dot	M	L
D_1	5.75 fF	1.5 pF	B_1	0.70 pH	71 pH
D_2	5.75 fF	1.5 pF	B_2	0.75 pH	73 pH
D_3	2.2 fF	1.75 pF	B_3	0.63 pH	68 pH
D_4	3.0 fF	1.9 pF	B_4	0.75 pH	78 pH
D_5	1.75 fF	0.84 pF	B_5	0.39 pH	40 pH

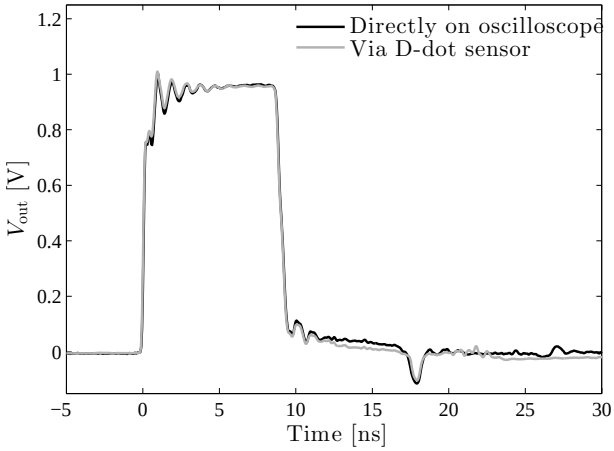

Fig. 8. Normalized D-dot voltage when the reed-relay pulse source is connected to the oscilloscope (at a lower voltage) and when the same pulse is measured by the D-dot sensor.

(which would not be true when the calibration is obtained from modeling results).

The output voltages of the B-dot sensors can be as high as several hundreds of volts when the nanosecond pulse source is operated at high voltages. The output voltages of the D-dot sensors are tens of volts and therefore significantly higher as compared with the first D-dot sensor in [4]. The penalty for this higher output voltage is that the frequency above which the sensors enter the self-integrating regime is now within the bandwidth that we need for our measurements. This can be seen in the transfer function of all the sensors in Fig. 7 as the bend in the straight line at around 2 GHz. However, because we carefully fitted the transfer function of the sensors, this is not a problem. Another potential disadvantage of the bigger sensors is that all sensor parameters are higher (bigger capacitances and inductances), which lowers the point at which the sensors can start to oscillate. However, as we can see from the measurements in Figs. 7a–c there are no oscillations visible, so the upper frequency limit of our sensors is at least 4 GHz. When we measured the S_{12} parameters of the sensors up to a higher frequency it seemed that the sensors started to oscillate in the 6–8 GHz frequency range, which is much higher than the frequency range we will operate the sensors in.

We tested all sensors with a reed-relay pulse source to verify the fitted transfer functions. This is a Blumlein pulse source which is switched by a mercury wetted reed-relay [28]. This pulse source is able to generate very fast pulses with a rise-time of several hundreds of picoseconds and a voltage amplitude of up to around 750 V. We performed one measurement at a charging voltage of 5 V with the output of the

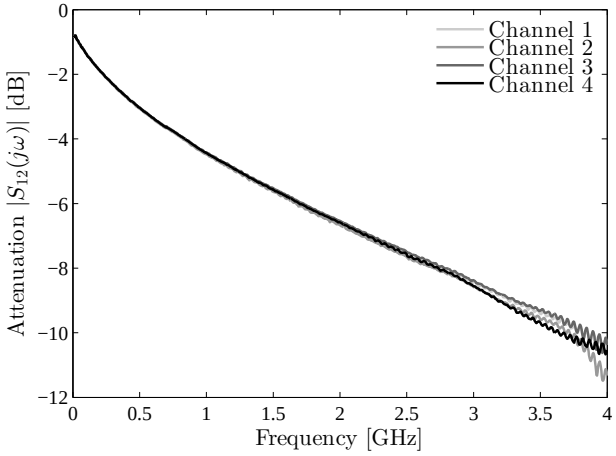

Fig. 9. Attenuation of the cables and connectors between the sensors and the oscilloscope, part of which are in the EMC cabinet. We used four cable systems (one each for each oscilloscope channel)

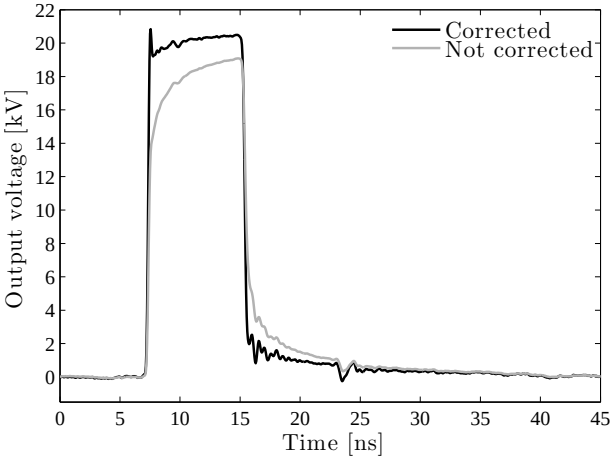

Fig. 10. Output voltage of the nanosecond pulse source for a 8-ns pulse as measured by the D-dot sensor when it is corrected and not corrected for the attenuation of the measuring cable assembly.

reed-relay pulse source connected directly to the oscilloscope. Then we generated the same pulse at a higher voltage, but now connected to the N-connector of Port 1 in Fig. 6. A 0–4 GHz 50 Ω load was connected at Port 3. The output of the sensor under test was captured by the oscilloscope (via a very short measuring cable) and numerically integrated using the inverse of the fitted transfer function from Fig. 7. Fig. 8 shows the normalized result together with the normalized result of the 5 V measurement directly on the oscilloscope for one of the D-dot sensors. The figure shows that we can measure correctly with this sensor. The results of the other sensors showed similar excellent agreement.

B. Measuring Cable Response

When the nanosecond pulse source is operated, all measuring equipment will be situated in an EMC cabinet [29]. Therefore, the sensors have to be connected by a long cable to the EMC cabinet. With the VNA, we measured the S_{12}-parameters of the entire cable assembly from the sensors to the oscilloscope, including the cable inside the EMC cabinet and all the adapters and connectors. Fig. 9 shows the results for four identical cable assemblies (one for each oscilloscope channel). It is clear that we have to correct for this attenuation.

Due to the BNC connectors on the oscilloscope the upper frequency limit of our cable assemblies is around 2 GHz, which is evident from the oscillations (and differences between the cable assemblies) that start above this frequency. Therefore, the upper frequency limit of our system is 2 GHz at the moment, but can be extended to 6–8 GHz (the upper frequency limit of the sensors themselves) if we would use connectors suited for higher frequencies in our cable assemblies and a suitable oscilloscope.

Fig. 10 shows the effect of the attenuation of the measuring cable attenuation on a measured 8-ns pulse from our nanosecond pulse source and what happens when we correct for it. Especially the high frequencies in the pulse are influenced, which results in a change of measured rise-time from 200 ps to 175 ps and a higher pulse amplitude when we correct for

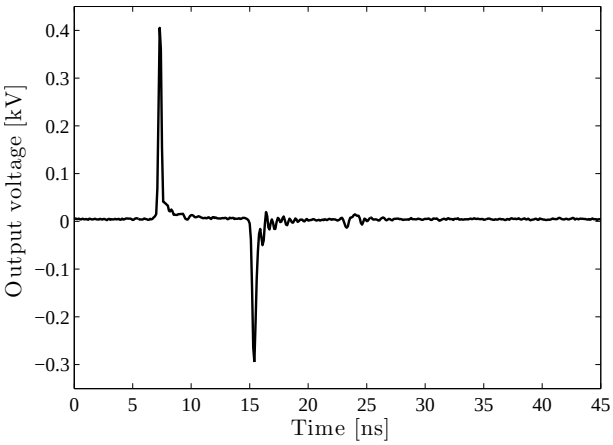

Fig. 12. The raw D-dot sensor signal as captured by the oscilloscope. It is the raw waveform for the results of Fig. 10.

the attenuation. Clearly, we need to correct for the attenuation. We implement this correction by transforming the measured signal to the frequency domain and dividing by the measured cable assembly S_{12} parameters, as we will show in the next part.

C. Total Measurement Setup

The total experimental setup and the numerical process that is used in all the measurements with the sensors is shown in Fig. 11 for a D-dot sensor (the method is the same for the B-dot sensors).

The oscilloscope (LeCroy 3-GHz 20-GS·s^{-1} WavePro 7300A[2]) captures the waveform from the D-dot sensor via an attenuator. The attenuator has a flat transfer function (within 0.05 dB of the specified value) up to at least 4 GHz (measured with the VNA). An example of a raw signal is shown in

[2]With the very short rise times of the nanosecond pulse source, we are operating the oscilloscope at the limit of its bandwidth. However, tests with a borrowed 30-GHz LeCroy oscilloscope confirmed that we can accurately measure the signals from the D-dot and B-dot sensors with the WavePro 7300A.

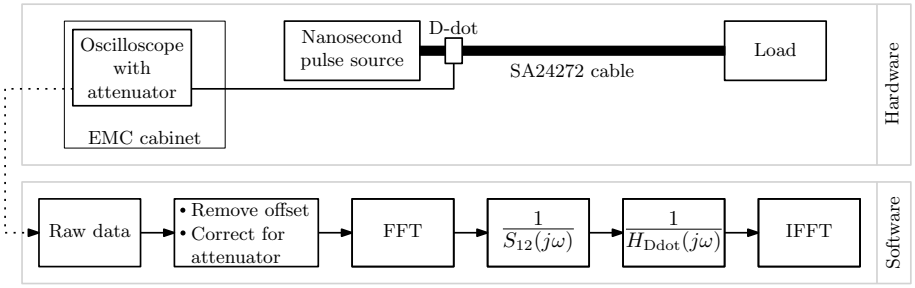

Fig. 11. The total experimental setup for the D-dot sensor measurements (the principle is the same for the B-dot sensor measurements). In the hardware part the voltage pulse is measured by the D-dot sensor with the oscilloscope. The raw waveform is then processed in software and corrected for the measuring cable attenuation ($S_{12}(j\omega)$) and the sensor transfer function of the sensor ($H_{\mathrm{Ddot}}(j\omega)$) in the frequency domain.

Fig. 12. It is the raw signal for the waveform shown in Fig. 10. This raw waveform is then processed in Matlab [30]. The first step is an offset correction and the correction for the attenuator. Then the signal is transformed to the frequency domain with the FFT (Fast Fourier Transform) where the cable correction with the inverse of the measured attenuation S_{12} (Fig. 9) is applied. Subsequently the inverse of the fitted transfer function of the D-dot sensor (Fig. 7) is applied before converting the signal back to the time domain with the inverse FFT (IFFT). The influence of the $\frac{1}{S_{12}(j\omega)}$-block was already shown in Fig. 10.

We process the results of the sensor signals numerically rather than passively in hardware because passive integrators at the high frequencies are very difficult to construct [31], [32]. Furthermore, using such a high-frequency passive integrator also requires the sensors to be perfectly differentiating up to a high-frequency. We already showed that this is not the case for our sensors.

D. Measurement Uncertainty

If we consider the entire setup, some measurement uncertainties are introduced. First, the BNC-connections on the oscilloscope introduce an estimated systematic uncertainty of up to 0.5%. Second, thermal expansion of the cables and the sensors introduce a variable (depending on the temperature) estimated uncertainty of up to 0.1%. Third, the uncertainty of the VNA measurement (introduced by the VNA itself, but also the fitting of the transfer functions) might be as high as 1%. Finally, the 8-bit vertical resolution of the oscilloscope introduces a further uncertainty of some percent. Whenever possible we use averaging of pulses to decrease the uncertainty of the oscilloscope, but the total estimated uncertainty introduced by the entire measurement setup can be as high as 5%. This uncertainty could be at least halved by using a higher resolution oscilloscope in future measurements.

V. Application Example: Energy Measurements

In this section we will shortly present an application example of the B-dot and D-dot sensors we developed.

One of the main challenges when applying the extremely short pulses from our nanosecond pulse source to a plasma reactor is to ensure that the energy from the pulses is efficiently transferred to the plasma. We studied this matching process in detail and the results are presented in [6], as well as in a future paper. For this matching study we used the B-dot and D-dot sensors to determine the energies in the system in detail.

With sensors D_5 and B_5 (refer to Fig. 5) we can measure the energy from the pulse source, but then we would only have two channels left on the 4-channel LeCroy WavePro 7300A oscilloscope for the plasma energy measurements and we specifically integrated two sensors of each type in each of the load-side sensor bodies to decrease the influence of interference on our measurements. Likewise, with sensors D_1, D_2, B_1 and B_2 we could measure the energy that is dissipated by the plasma, but have no channels left to measure the supplied energy by the nanosecond pulse source. The solution to this problem is the use of sensors D_3, D_4, B_3 and B_4. We purposely situated these sensors at a distance from the reactor such that we can measure the incoming pulse as it arrives and then measure the reflected pulse from the reactor with enough time interval between these pulses (even at the 10-ns pulse duration setting of the pulse source). In this way we can calculate the plasma energy as the incoming energy minus the reflected energy.

Figure 13 shows an example of an energy measurement, starting with the measured voltage and current with sensors D_3–D_4 and B_3–B_4 respectively in Fig. 13a. By using this sensor position we can first see the complete 5-ns incident pulse from the pulse source passing (notice that this would still be the case for a 10-ns pulse). Figures 13b and 13c show the corresponding power and energy calculated from these waveforms.

The power and energy are calculated from the D-dot and B-dot sensors with:

$$\mathrm{Power}(t) = I_{\mathrm{B}_{3-4}}(t) V_{\mathrm{D}_{3-4}}(t). \tag{8}$$

$$\mathrm{Energy}(t) = \int_0^t \mathrm{Power}(\tau)\, d\tau. \tag{9}$$

We see in Fig. 13c that we can measure the total applied energy to the reactor E_{tot} by taking only the contribution of the first incident pulse.

When the pulse passes the sensor position it encounters the reactor and will partly reflect back to the pulse source and partly transmit into the reactor (the plasma reactor is a coaxial structure with a thin wire as the central electrode and a solid metal grounded cylinder as the outer electrode). The vacuum

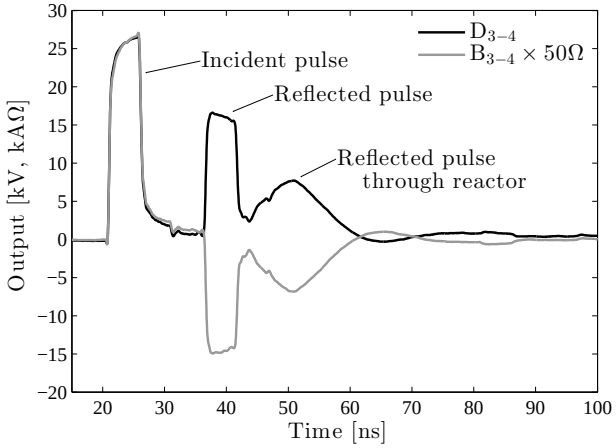

(a)

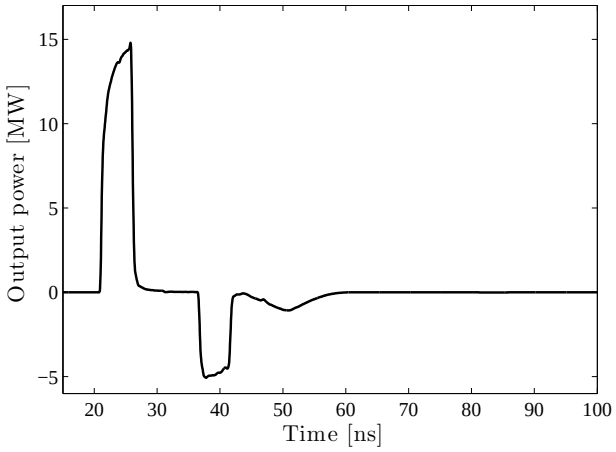

(b)

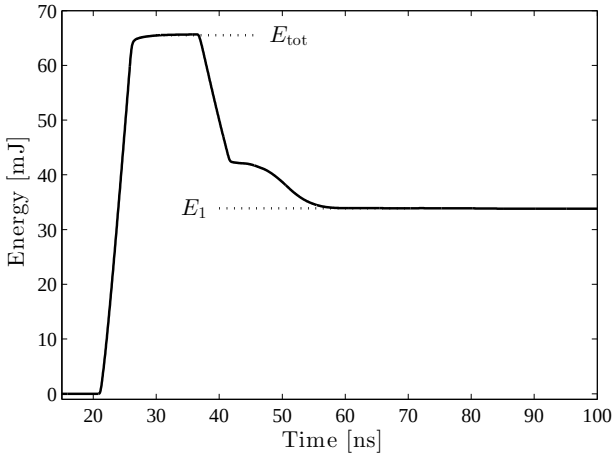

(c)

Fig. 13. Example of an energy measurement with the D-dot and B-dot sensors. (a) Voltage and current measured with sensors D_3–D_4 and B_3–B_4 respectively. We see the incident pulse and its reflection on the plasma reactor as well as the attenuated pulse that traveled up and down the reactor. (b) The power of the pulse in (a). (c) The energy calculated from the power in (b).

impedance of the reactor is higher than the cable impedance, so the reflected pulse will be positive. This is the reflected pulse as indicated in Fig. 13a.

The part of the pulse that is transmitted into the reactor propagates up and down the reactor, generating plasma, and transmits back into the SA24272 cable. This is the third, attenuated peak in Fig. 13a. It is severely attenuated and dispersed by the plasma. Part of the pulse inside the reactor will also reflect back into the reactor instead of transmitting into the SA24272 cable, but this part diminishes over time.

If we look at Fig. 13c then we see that the reflected pulse causes a sharp decrease in energy because the energy of the reflected pulse moves in the opposite direction of the incident pulse. This opposite direction is also apparent from the current in Fig. 13a. The attenuated pulse from the reactor decreases the energy even more. After this time the energy is stable. The energy that is measured at this point is the energy that is 'left' in the reactor and is therefore the energy that was dissipated by the plasma. This energy is indicated by E_1. We can now use E_{tot} and E_1 to calculate the efficiency of the energy transfer of the pulses to the plasma.

We can perform all the energy measurements with just one sensor body. This allows for the use of two D-dot sensors and B-dot sensors for all measurements. This would not have been possible with sensors D_1, D_2, B_1 and B_2.

VI. Summary and Conclusions

In this paper, we presented a large-bandwidth, high-current and high-voltage measuring system for pulse measurements in pulsed power systems. The sensors can be easily calibrated, require no extensive (3D) modeling, are very compact, are inexpensive, and have a bandwidth of up to several GHz. Moreover, they can be used in any pulsed power system where a pulse source is connected to its load by a coaxial cable (without disturbing the coaxial geometry).

We developed these sensors for use with our nanosecond pulse source system. The type of sensors we used are D-dot and B-dot sensors that are able to measure the voltage and current through capacitive coupling and inductive coupling respectively. For implementing these sensors we take advantage of the option to compactly mount them on the SA242727 cable that connects our nanosecond pulse source to its load. This enables us to measure the characteristics of each sensor very precisely with a vector network analyzer. With these characteristics we can numerically reconstruct the voltage and current waveforms that passed the sensor positions.

We have three sensor bodies in total: two bodies with two D-dot sensors and two B-dot sensors each near the load and one sensor body with one of each type of sensor at the end of the nanosecond pulse source. The employ of two sensors of each type at the load side results in a lower influence of oscilloscope noise and interference. The interference was further reduced by using a differential B-dot system and by designing the sensors in such a way that their output voltage is high compared to the interference.

Calibration of the D-dot sensors and B-dot sensors showed that the sensors are not purely working in the differentiating regime. However, because we were able to measure the transfer function of the sensors with the vector network analyzer, this presented no issue. Furthermore, we showed a measurement approach that partly relies on numerical processing. In this process we have to correct for the measuring cable and

the transfer function of the D-dot and B-dot sensors to obtain very accurate results.

Finally, while we used the sensors for energy measurements, camera triggering and the general measurement of the pulses, other researchers can use these type of sensors as well in any system where a (coaxial) cable connects a pulse source to its load.

REFERENCES

[1] H. Bluhm, *Pulsed Power Systems: Principles and Applications*. Springer, 2006.

[2] S. J. Voeten, "Matching high voltage pulsed power technologies," Ph.D. dissertation, Eindhoven University of Technology, 2013, Available online: http://alexandria.tue.nl/extra2/750268.pdf.

[3] T. Huiskamp, S. J. Voeten, E. J. M. van Heesch, and A. J. M. Pemen, "Design of a subnanosecond rise time, variable pulse duration, variable amplitude, repetitive, high-voltage pulse source," *Plasma Science, IEEE Transactions on*, vol. 42, no. 1, pp. 127–137, 2014.

[4] T. Huiskamp, F. J. C. M. Beckers, E. J. M. van Heesch, and A. J. M. Pemen, "First implementation of a subnanosecond rise time, variable pulse duration, variable amplitude, repetitive, high-voltage pulse source," *Plasma Science, IEEE Transactions on*, vol. 42, no. 3, pp. 859–867, 2014.

[5] T. Huiskamp, E. J. M. van Heesch, and A. J. M. Pemen, "Final implementation of a subnanosecond rise time, variable pulse duration, variable amplitude, repetitive, high-voltage pulse source," *Plasma Science, IEEE Transactions on*, vol. 43, no. 1, pp. 444–451, 2015.

[6] T. Huiskamp, "Nanosecond pulsed power technology for transient plasma generation," Ph.D. dissertation, Eindhoven University of Technology, 2015, Available online: http://alexandria.tue.nl/extra2/798746.pdf.

[7] T. Huiskamp, H. Höft, M. Kettlitz, and A. J. M. Pemen, "Visualization of a spark discharge driven by a high-voltage pulse with sub-ns rise-time at atmospheric pressure," *Plasma Science, IEEE Transactions on*, vol. 42, no. 10, pp. 2414–2415, 2014.

[8] H. Höft, T. Huiskamp, M. Kettlitz, and A. J. M. Pemen, "Visualization of a coaxial dielectric barrier discharge driven by a sub-ns rising high-voltage pulse and its reflections," *Plasma Science, IEEE Transactions on*, vol. PP, no. 99, pp. 1–1, 2014.

[9] C. Waters, "Current transformers provide accurate, isolated measurements," *Power conversion & intelligent motion*, no. 12, 1986.

[10] J. Bergoz, "Current monitors for particle beams," *Nuclear Physics A*, vol. 525, pp. 595–600, 1991.

[11] P. Ripka, "Electric current sensors: a review," *Measurement Science and Technology*, vol. 21, no. 11, p. 112001, 2010.

[12] "North Star High Voltage," http://www.highvoltageprobes.com/high-voltage-probes, accessed: 01-08-2015.

[13] W. Rogowski and W. Steinhaus, "Die messung der magnetischen spannung," *Electrical Engineering (Archiv fur Elektrotechnik)*, vol. 1, no. 4, pp. 141–150, 1912.

[14] D. G. Pellinen and P. W. Spence, "A nanosecond risetime megampere current monitor," *Review of Scientific Instruments*, vol. 42, no. 11, pp. 1699–1701, 1971.

[15] J. M. Anderson, "Wide frequency range current transformers," *Review of Scientific Instruments*, vol. 42, no. 7, pp. 915–926, 1971.

[16] E. H. W. M. Smulders, B. E. J. M. Van Heesch, and S. S. V. B. van Paasen, "Pulsed power corona discharges for air pollution control," *Plasma Science, IEEE Transactions on*, vol. 26, no. 5, pp. 1476–1484, Oct 1998.

[17] A. P. J. van Deursen and V. Stelmashuk, "Inductive sensor for lightning current measurement, fitted in aircraft windowspart I: Analysis for a circular window," *IEEE Sensors Journal*, vol. 11, no. 1, p. 199, 2011.

[18] A. P. van Deursen, "Inductive sensor for lightning current measurement, fitted in aircraft windowspart II: Measurements on an A320 aircraft," *IEEE Sensors Journal*, vol. 11, no. 1, pp. 205–209, 2011.

[19] B. M. Novac, M. Ganciu, M. C. Enache, I. R. Smith, H. R. Stewardson, and V. V. Vadher, "A fast electro-optic high-voltage sensor," *Measurement Science and Technology*, vol. 6, no. 2, p. 241, 1995.

[20] R. D. Shah, R. J. Cliffe, B. M. Novac, I. R. Smith, and P. Senior, "An ultra-fast electro-optic probe for 500 kV pulsed voltage measurements," *Measurement Science and Technology*, vol. 13, no. 2, p. 226, 2002.

[21] A. Lorusso, V. Nassisi, and M. V. Siciliano, "Fast capacitive probe for electromagnetic pulse diagnostic," *Review of Scientific Instruments*, vol. 79, no. 6, pp. 064 702–064 702, 2008.

[22] T. C. Wagoner, W. A. Stygar, H. C. Ives, T. L. Gilliland, R. B. Spielman, M. F. Johnson, P. G. Reynolds, J. K. Moore, R. L. Mourning, D. L. Fehl *et al.*, "Differential-output B-dot and D-dot monitors for current and voltage measurements on a 20-MA, 3-MV pulsed-power accelerator," *Physical Review Special Topics-Accelerators and Beams*, vol. 11, no. 10, p. 100401, 2008.

[23] C. Yao, Q. Xiao, Y. Mi, T. Yuan, C. Li, and W. Sima, "Contactless measurement of lightning current using self-integrating B-dot probe," *Dielectrics and Electrical Insulation, IEEE Transactions on*, vol. 18, no. 4, pp. 1323–1327, 2011.

[24] A. G. A. Lathouwers, "Ontwerp van een differentiërend-integrerend meetsysteem voor het meten van snelle transiënte spanningen in GIS (in Dutch)," Master's thesis, Eindhoven University of Technology, 1988.

[25] M. A. van Houten, "Electromagnetic compatibility in high-voltage engineering," Ph.D. dissertation, Eindhoven University of Technology, 1990.

[26] R. H. Huddlestone and S. L. Leonard, "Plasma diagnostic techniques," in *Plasma Diagnostic Techniques*, 1965.

[27] W. Stygar and G. Gerdin, "High frequency rogowski coil response characteristics," *Plasma Science, IEEE Transactions on*, vol. 10, no. 1, pp. 40–44, 1982.

[28] P. W. Smith, *Transient electronics: Pulsed circuit technology*. J. Wiley, 2002.

[29] E. J. M. van Heesch, J. N. A. M. van Rooij, R. G. Noij, and van der Laan P. C. T, "A new current and voltage measuring system; tests in a 150 kv and 400 kv GIS," in *Proc. 5th Int. Symp. on High Voltage Engineering*, vol. 3, 1987, p. 73.06.

[30] "MathWork Matlab," http://www.mathworks.com/products/matlab/, accessed: 01-08-2015.

[31] M. Raleigh and R. E. Pechacek, "Fast passive integrator," *Review of scientific instruments*, vol. 55, no. 12, pp. 2023–2026, 1984.

[32] V. Stelmashuk and A. P. J. van Deursen, "Passive integrator for ILDAS project," in *EMC Europe 2011 York*. IEEE, 2011, pp. 37–40.

T. Huiskamp was born in Den Dolder, The Netherlands, in 1985. He received his M.Sc degree (with honors) and Ph.D degree (with honors) in electrical engineering from Eindhoven University of Technology (TU/e), Eindhoven, The Netherlands, in 2011 and 2015 respectively. His Master's thesis was on the application of pulsed power to InnoPhysics' PlasmaPrint technology. As a Ph.D Researcher, he worked on nanosecond pulsed power induced corona plasmas at the Electrical Energy Systems Group of Eindhoven University of Technology, where he currently works as a postdoctoral researcher.

F. J. C. M. Beckers was born in Tegelen, The Netherlands, in 1982. He received his M.Sc. degree and Ph.D degree in electrical engineering from Eindhoven University of Technology in 2008 and 2015 respectively. Since 2008 he was employed at HMVT-Antea as pulsed power engineer. In 2011 he also joined the Electrical Energy Systems group at Eindhoven University of Technology as a Ph.D. researcher. His work focused on high power repetitive pulsed corona plasma generation for industrial scale gas-cleaning applications. Currently, he is a postdoctoral researcher in the same group.

E. J. M. van Heesch was born in Utrecht, The Netherlands, in 1951. He received the Master's degree in physics from the Eindhoven University of Technology, The Netherlands, and the Ph.D. degree in plasma physics and fusion related research from the University of Utrecht, The Netherlands, in 1975 and 1982, respectively. Since 1986, he has been an Assistant Professor at the Eindhoven University of Technology. Here, he is leading pulsed power research. He was previously involved with shocktube gas dynamics (Eindhoven, 1975) and with fusion technology (Jutphaas, The Netherlands, 1975-1984, Suchumi former USSR, 1978 and Saskatoon, Canada, 1984-1986). Among his designs are various plasma diagnostics, a toroidal fusion experiment, substation high-voltage measuring systems and systems for pulsed-power processing. He organizes many projects with industry and national and European Union research agencies. His research is the basis for teaching and coaching university students and Ph.D. candidates. He is a co-inventor of several patents and has (co-)authored more than 200 publications.

A. J. M. Pemen (M'98) received the B.Sc. degree from the College of Advanced Technology, Breda, The Netherlands, in 1986 and the Ph.D. degree in electrical engineering from the Eindhoven University of Technology, The Netherlands, in 2000, both in electrical engineering. Before joining the Electrical Energy Systems Group (EES), Eindhoven University of Technology in 1998 as an Associate Professor, he was with KEMA, Arnhem, The Netherlands. He is associated professor on pulsed-power and pulsed plasma technology. His research interest includes high-voltage engineering, pulsed-power, plasmas, and renewable energy systems. Among his achievements are the development of an on-line monitoring system for partial discharges in turbine generators, a pulsed-corona system for industrial applications, and a pulsed corona tar cracker. He is the Founder of the Dutch Generator Expertise-Center.